Published online May 17, 2018

Original Research

Core Ideas

- A novel coupled inversion algorithm estimated soil and root parameters.
- Electrical resistivity data were used to identify root and soil hydraulic properties.
- A unique root distribution was estimated despite input error and data density.
- This noninvasive technique can capture root dynamics in a variety of settings.

Quantifying Soil Water and Root Dynamics Using a Coupled Hydrogeophysical Inversion

Alexandria S. Kuhl,* Anthony D. Kendall, Remke L. Van Dam, and David W. Hyndman

Plot- to field-scale root distribution data are relatively rare and difficult to measure with traditional methods. Nevertheless, these data are needed to accurately model root water uptake (RWU) processes within agronomic, hydrologic, and terrestrial biosphere models. New tools are needed to effectively observe root distributions and model dynamic root growth processes. In the past decade, geophysical tools have increasingly been used to study the vadose zone, and hydrogeophysical inversions have shown promise to noninvasively characterize water dynamics. In such an approach, the hydrology is modeled and hydrological data are inverted with the geophysical data, constraining the geophysical inversion results and decreasing uncertainty and the number of nonunique solutions. In this study, we developed and tested a coupled hydrogeophysical inversion approach that uses electrical resistivity data to estimate soil hydraulic, petrophysical, and root dynamic parameters. This builds on prior research that used either a coupled hydrogeophysical inversion to estimate soil hydraulic parameters only, or a hydrological inversion to estimate root distribution or root water uptake parameters. Our results indicate that under the conditions tested, this approach accurately captures root water dynamics and soil hydraulic parameters. This opens up opportunities to noninvasively image a variety of root distributions and soil systems, better understand the dynamics of RWU processes, and improve estimates of transpiration for systems models.

Abbreviations: DD, data density; ER, electrical resistivity; PP, petrophysical parameters; MRD, maximum rooting depth, RP, root parameters; RWU, root water uptake; SC, site characterization; SHP, soil hydraulic parameters.

A.S. Kuhl, A.D. Kendall, R.L. Van Dam, D.W. Hyndman, Dep. of Earth and Environmental Sciences, Michigan State Univ., East Lansing, MI 48824; R.L. Van Dam, Dep. of Civil Engineering, Centro Federal de Educação Tecnológica de Minas Gerais, CEP 30510-000, Belo Horizonte, Brazil. *Corresponding author (kuhlalex@msu.edu).

Received 23 Aug. 2017.
Accepted 1 Jan. 2018.
Supplemental material online.

Citation: Kuhl, A.S., A.D. Kendall, R.L. Van Dam, and D.W. Hyndman. 2018. Quantifying soil water and root dynamics using a coupled hydrogeophysical inversion. Vadose Zone J. 17:170154. doi:10.2136/vzj2017.08.0154

Transpiration is the most important pathway for the exchange of water from Earth to the atmosphere, accounting for up to 80% of terrestrial evapotranspiration (Jasechko et al., 2013). Thus, disruptions to the plant community through climate and land-use changes will likely have serious implications for regional to global water balances. To predict and mitigate the effects of those changes, agronomic, hydrologic, and terrestrial biosphere models must accurately capture the exchange of water along transpiration pathways. Doing so requires understanding the underlying processes that drive such exchanges. The interdependent and dynamic nature of the factors controlling transpiration, and our inability to observe the processes directly, makes transpiration challenging to appropriately represent in these models.

Transpiration is fundamentally controlled by root distributions and root water uptake (RWU) processes, yet due in part to a lack of dynamic root function data, these processes are often oversimplified in models (Warren et al., 2015). Such data are rarely available because it is challenging to observe roots in the field, especially changes with time (Cai et al., 2018). Direct approaches such as excavation and root windows are limited at the field scale and are very costly and labor intensive. These approaches are also not as feasible for deep roots associated with woody plants, such as trees (Maeght et al., 2013). Nondestructive methods are thus needed to understand plant functions as a response to changing conditions in a range of field settings. One viable approach is to use changes in root-zone soil moisture as a proxy for the presence of RWU processes.

Existing methods to measure or estimate changes in soil moisture have limitations. Larger scale methods that rely on measuring atmospheric fluxes, such as eddy covariance, can get measurements at the stand level, but it is difficult to isolate transpiration from evaporation fluxes. Belowground, tools such as time domain reflectometry, neutron probes, and capacitance probes estimate soil moisture with high temporal resolution, but they are intrusive, and barring significant installation efforts, lack the necessary spatial resolution to capture heterogeneities in soil properties and root densities. Lysimeters can measure the drainage out of the profile but are costly and labor intensive and cannot capture sublayer dynamics (Schelle et al., 2012).

Electrical resistivity (ER), a minimally invasive geophysical technique, measures the current-induced potential field underground. Electrical resistivity data, comprised of measured potentials at varying dipole lengths and distances, are strongly influenced by not only the porosity of the soil but also the saturation and electrical conductance of the pore water. A petrophysical relationship equates these variables to the bulk resistivity calculated from the measured potentials (Archie, 1942). Thus, if the resistivity and pore water conductivity are known, soil moisture can be estimated via empirical relationships fit with petrophysical parameters (PP). Electrical resistivity surveys are particularly well suited to investigate hydrological problems because they provide a bulk measurement influenced by a volume of media surrounding the electrodes, the dimension of which can be varied with the electrode array geometry. For example, an ER survey could be designed to have increased sensitivity to the upper 0.5 m where most RWU activity is concentrated. For contrast, traditional discrete methods of sampling soil moisture represent conditions at a single point and are susceptible to both over- and under-representation of volumetric soil moisture due to features such as textural layering and macropores. Further, the behavior of current flow makes it ideal to study the subsurface in multiple dimensions, unlike point measurements that require a large installation effort to capture lateral variability.

Previous research has used the relationship between ER and soil moisture to infer the presence of roots and RWU dynamics in multiple dimensions and at high spatial and temporal resolutions (e.g., Michot et al., 2003; Jayawickreme et al., 2008, 2010; Garré et al., 2011, 2013; Robinson et al., 2012; Beff et al., 2013; Ma et al., 2014; Fan et al., 2015; Bass et al., 2017; Whalley et al., 2017). These studies applied a traditional ER inversion method to retrieve the soil moisture distribution, wherein a potential field model is optimized to fit the measured potentials from the ER survey and translated to a static soil moisture distribution via a petrophysical relationship. However, such traditional ER data inversions may result in nonunique and unconstrained solutions and produce physically unrealistic soil moisture distributions (Mboh et al., 2012).

To improve the application of ER methods to hydrological problems, researchers have proposed coupling the geophysical model with a site-specific hydrological model (Hinnell et al., 2010; Minsley et al., 2011; Singha et al., 2015). One approach to coupled hydrogeophysical inversion involves (i) forward modeling transient water fluxes, (ii) converting the final modeled soil moisture distribution into an ER distribution using a petrophysical relationship, (iii) forward modeling the potential field to compare the modeled and measured potentials, and then (iv) updating coupled model parameters to minimize differences between the observed and modeled ER data (Mboh et al., 2012). In such an approach, changes to the soil hydraulic parameters affect the soil moisture distribution via the hydrologic model; this change in simulated soil moisture alters the modeled electrical potential field.

There are three categories of parameters that are typically unknown in near-surface hydrogeophysical problems: petrophysical parameters (PP), soil hydraulic parameters (SHP), and root parameters (RP). The PP describe the relationship between simulated soil moisture and subsurface ER. The SHP affect the soil water dynamics via water retention and infiltration models. The RP control modeled root physiology, including the growth and distribution of the roots, along with the relationships among potential transpiration, soil moisture, and RWU.

Several studies have used a coupled hydrogeophysical inversion approach to successfully estimate SHP and transient soil moisture in both synthetic (Hinnell et al., 2010) and field (Mboh et al., 2012; Moreno et al., 2015; Tran et al., 2016; Thomas et al., 2017) scenarios. Mboh et al. (2012) used ER data from a short (several hour) inflow experiment to estimate SHP. They found the ER data-only inversion more robust than just using cumulative inflow data and slightly worse than combining both data types in the objective function. Despite this, ER data without supporting hydrological data have been demonstrated to be sensitive enough to soil moisture dynamics to reasonably estimate SHP. Using a grain-size analysis and the Rosetta database (Schaap et al., 2001) to initialize the SHP, Moreno et al. (2015) used nine geophysical surveys throughout a year-long period to fit select SHP in a two-layer soil. The RP in this particular study were fixed (held constant) at reference values.

Despite the interest in this area of research, few if any studies have attempted to use a coupled hydrogeophysical inversion approach to characterize RWU dynamics. Root water uptake models that include the root distribution and water stress functions for RWU reduction have, to our knowledge, been parameterized with root or hydrological data inversions only. Hupet et al. (2003) used neutron probe water content data to estimate model parameters, including SHP for a one-dimensional homogeneous soil, and rooting depth and root length density for a maize (*Zea mays* L.) crop with mixed success; the RP were less well constrained in medium-textured soils. Schelle et al. (2012) completed a similar study, using daily lysimeter and matric potential data to estimate SHP in two layers, as well as a root distribution parameter. Using neutron probe soil moisture data, Vrugt et al. (2001) calibrated multiple parameters of a new flexible two-dimensional root distribution model and some SHP, with excellent agreement between measured and modeled soil moisture in two dimensions. Recently, Cai et al. (2018) demonstrated the use of a similar method to

parameterize several different water stress functions for one-dimensional RWU to fit field observations of daily water content, with good agreement between modeled and observed root length density distributions.

Prior studies have provided convincing evidence that, separately, (i) RWU models can be parameterized using inverted water content data (e.g., Hupet et al., 2003), and (ii) ER data can serve as a proxy for water content data and can be used to estimate SHP (e.g., Hinnell et al., 2010). Therefore, we hypothesized that RWU models can be parameterized in a coupled hydrogeophysical inversion using ER data, which to date has not been directly investigated. To test this hypothesis, we developed a method that builds on these two established concepts by estimating SHP and RP using a coupled hydrogeophysical inversion of ER data. We also incorporated the estimation of PP in the relationship between soil moisture and resistivity. Given the challenges posed by the lack of transient root data from the field, we sought to validate this novel approach with a synthetic one-dimensional proof-of-concept study. In addition to validating the method, we sought to identify the limitations that sparse data and parameter measurements and sensitivity errors might impose on this approach.

Informing the ER data with the known hydrology of the site reduces the nonunique solutions to only those that match a physical reality. Additionally, when soil water fluxes are modeled, losses from evaporation can be distinguished from transpiration as well as hydraulic redistribution. This is a particular benefit over time-differential ER methods, which can only provide total gains or losses in soil moisture. Furthermore, the embedded hydrological model can then be used to simulate soil moisture conditions prior to, between, and after ER survey events. Using ER methods in this fashion to calibrate a process-based model also allows the model to be used to forecast soil moisture fluxes under hypothetical future climate conditions.

As with standard ER inversions, however, the petrophysical relationship must be known, which remains a challenge to any geophysical approach used to estimate hydraulic properties (Laloy et al., 2011). In addition, the behavior of some SHP parameters is not independent of others, making it difficult to estimate a full spatial distribution of values. Roots themselves can also affect the ER signal; however, this has primarily been shown for much larger tree roots, whose resistance is distinguishable from the surrounding material (Amato et al., 2008). While there are added complexities with real field settings related to lateral heterogeneity, this does not necessarily preclude the establishment of a representative hydrological model.

In this study, we established a framework for a robust, minimally invasive, and cost- and labor-efficient way to calibrate the many parameters of site-specific hydrological models. We present an overview of the model components used to build the algorithm, test the sensitivity of the parameters, and perform a series of synthetic one-dimensional modeling experiments to validate the algorithm. To ensure that the synthetic study reflects realistic conditions, we used climate data and measured soil profile characteristics from a study site at the Kellogg Biological Station in southwestern Michigan, described in more detail below. The approach detailed here is universally applicable and provides a path to investigate heterogeneous root and soil systems in two and three dimensions with limited a priori information.

Materials and Methods

We developed a coupled hydrogeophysical inversion algorithm that (i) simulates the movement of water throughout the soil profile, (ii) converts snapshots of the transient soil moisture distribution to soil resistivity using a petrophysical relationship, (iii) simulates the potential field and ER data using a forward resistivity model, and (iv) optimizes the parameters of the models by minimizing the difference between the modeled and measured ER data. This approach can estimate the SHP, RP, and PP that are often challenging to directly measure either in situ or with laboratory bench experiments.

Our algorithm simulates the hydrogeophysical processes using four publicly available codes (Fig. 1): the System Approach to Land Use Sustainability (SALUS) model (Basso et al., 2006) for potential evaporation and transpiration; HYDRUS (Šimůnek et al., 2005) for root growth (Hartmann et al., 2018), RWU (Feddes et al., 2001), hydraulic redistribution, variably saturated hydrology (Richards, 1931), snow hydrology, and heat transport (Chung and Horton, 1987); FWD2_5D (Pidlisecky and Knight, 2008) for the electrical potential forward calculations; and the global optimization Shuffled Complex Evolution Algorithm, SCE-UA (Duan et al., 1992) for parameter estimation. Each of these four models and algorithms are described in more detail below.

To demonstrate and validate this inversion algorithm, our experiment involved three steps in which we (i) forward ran the algorithm with a set of reference parameters to generate a reference hydrological model and synthetic "measured" ER data, (ii) tested the objective function sensitivity to SHP, PP, RP, and (iii) tested the inversion algorithm under six scenarios that tested the influence of variations in data density and parameter uncertainty. We evaluated each of the six inversion results relative to the synthetic reference parameters, soil moisture, root distribution, and RWU data.

Reference Model

We developed a realistic plot-scale one-dimensional vertical model of maize in a three-layer soil, assuming uniform soil and root properties laterally (Fig. 2). We based this model on a test plot at the Kellogg Biological Station Great Lakes Bioenergy Research Center site in southwestern Michigan (described previously by Zenone et al., 2013). Actual data from this site for climate conditions, sediment grain size distributions, soil moisture, soil temperature, and petrophysical relationships were used for this synthetic model. This plot was also instrumented with electrodes for ER surveys to be used in future studies.

Hydrological modeling was conducted in HYDRUS, which solves Richards' equation for unsaturated flow. Some HYDRUS

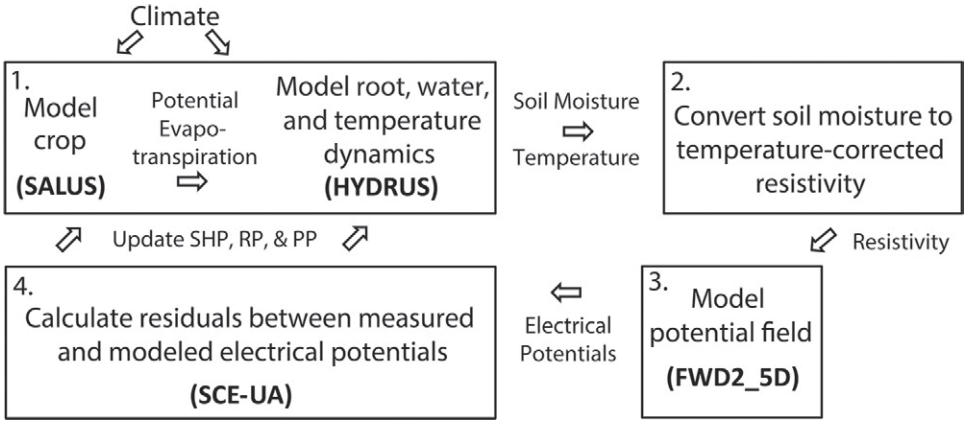

Fig. 1. Schematic of the four-step coupled hydrogeophysical inversion algorithm that estimates petrophysical parameters (PP), soil hydraulic parameters (SHP), and root parameters (RP) to minimize the root mean square error (RMSE) between measured and modeled electrical potentials. Boxes contain the components of the algorithm, while labeled arrows describe the flow of output from one component to the other. Model codes used include the System Approach to Land Use Sustainability crop model (SALUS), a one-dimensional hydrological model (HYDRUS), an electrical resistivity forward model (FWD2_5D), and a Shuffled Complex Evolution optimization model developed at the University of Arizona (SCE-UA).

inputs, including potential evaporation and potential transpiration, were estimated using the SALUS crop model (Basso et al., 2006) and imported to HYDRUS. The SALUS model is a daily water and nutrient balance dynamic vegetation model that uses daily climate data to calculate potential evapotranspiration using the Priestley–Taylor equation. It also models the leaf area index to differentiate evaporation from transpiration (Ritchie, 1998). Daily values of potential evapotranspiration were disaggregated proportional to the hourly modeled sun position obtained from the MATLAB File Exchange and validated using NOAA's Solar Calculator. HYDRUS was selected over SALUS for modeling RWU along with water and energy fluxes because while SALUS computes daily temperature and water balance within the root zone, HYDRUS has a finer vertical discretization and incorporates a more sophisticated hydrology algorithm. Daily soil moisture output from SALUS was also deemed insufficient due to the sensitivity of ER to diurnal changes in soil moisture (Robinson et al., 2012).

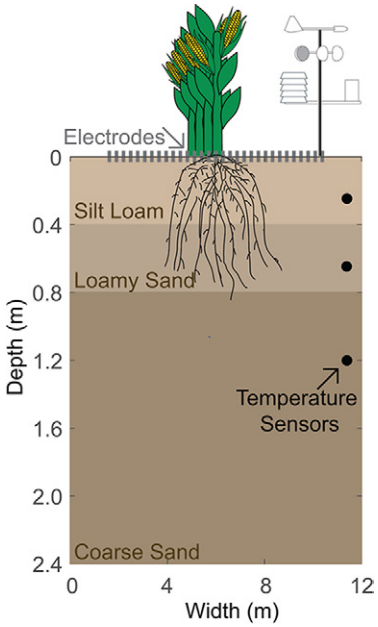

Fig. 2. Schematic diagram of the model profile with soil layers and plant roots overlain by a local weather station (with air temperature, wind speed, solar radiation, and precipitation), three buried temperature sensors, and 30 electrodes.

For the purposes of the study, we assumed no error in the climate data inputs, soil temperature, leaf area index, potential evapotranspiration calculation, or soil layer boundaries. We assumed that hydraulically significant soil layering could be accurately identified from in situ textural classification, and that for this plot-scale study, these layer boundaries are horizontal. However, the model could be adapted to estimate layer boundaries by allowing layer depths to vary. Weather stations are widely available at high spatial resolutions, making it easier to model temperature dynamics and potential evapotranspiration. Crop models that focus on modeling yield such as SALUS are also well suited to modeling the leaf area index.

We chose to describe the root distribution in HYDRUS with the Vrugt model (Vrugt et al., 2001) because of its flexibility. The parameters of the reference Vrugt model were estimated to fit the normalized root distribution output from SALUS at the end of the growing season using an unconstrained nonlinear optimization (Fig. 3). The Vrugt model is

$$\text{beta} = \frac{1-x}{\text{MRD}} \exp\left(\frac{-\text{pz}}{\text{MRD}}|\text{zv}-x|\right) \quad [1]$$

where x is depth, MRD is the "maximum" rooting depth at which the root density becomes zero, and pz and zv are fitting parameters that alter the rate of exponential decay and set the depth of the MRD, respectively. A smooth exponential root distribution can be obtained by setting zv to zero. The calibrated root distribution (pz = 5 and MRD = 1.0 m, Fig. 3) is similar to the root density distributions observed for maize (Tardieu, 1988;

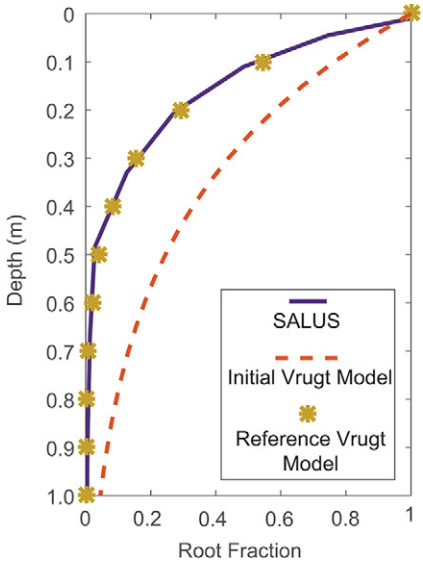

Fig. 3. The Vrugt equation (Eq. [1]) solved for depths up to 1.0 m with the perturbed initial parameters (orange dashed line) vs. those parameterized to fit the output from the SALUS model (yellow stars). Note that the dependent variable is on the *x* axis.

Jackson et al., 1996). Because the decay of the exponential root distribution is largely dependent on the pz/MRD ratio (Eq. [1]), we estimated only pz in the optimization. An analysis of different pz and MRD values found that multiple combinations could closely replicate the observed root distribution. Assuming that the MRD value would not be known in reality, and it is the pz/MRD ratio that primarily influences the shape of the curve, MRD was fixed at 1.5 m for the tested scenarios. Although we chose the Vrugt root distribution model, any of the four root distribution models available in the HYDRUS root growth module could be parameterized with this coupled inversion algorithm. In addition, the models could be within the search space of the optimization, allowing even greater flexibility.

The Feddes model (Feddes et al., 2001) was used in HYDRUS to simulate the reduction of potential transpiration during periods of water stress, which occur when the soil moisture is outside of a prescribed range. Water stress in the Feddes model is determined by four pressure head thresholds: h_1, h_2, h_3, and h_4. In the ideal pressure head range, between h_2 and h_3, water is extracted at the potential transpiration rate. When the pressure head is beyond the ideal range, (above h_2 or below h_3), the potential transpiration is proportional to the increase or decrease in pressure head. Beyond the pressure head limits for water extraction, h_1 and h_4, the reduction coefficient is 0, resulting in zero RWU. The parameter h_2 can be dependent on the texture of the soil, while h_3 can have an upper and lower threshold (denoted with a subscript H or L, respectively). Reference values of RP for maize, h_1, h_2 (soil-layer dependent), h_{3H}, h_{3L}, and h_4 (Supplemental Table S2) were taken from Wesseling et al. (1991).

Grain size analysis from samples at the site provided sand, silt, and clay contents and bulk density at 0.1-m intervals. From this analysis, three distinct layers and the boundary locations between them were identified at 0.4 and 0.8 m. The soils are described as well-drained Alfisols with a silt loam layer over loamy sand, underlain by coarse sand (Fig. 2). The soil is classified as a Typic Hapludalf. The van Genuchten–Mualem model (van Genuchten, 1980) was implemented in HYDRUS to model soil water retention and infiltration:

$$\theta(h)=\theta_r+(\theta_s-\theta_r)\left(1+|\alpha h|^n\right)^{-m} \quad [2]$$

$$S_e(h)=\frac{\theta(h)-\theta_r}{\theta_s-\theta_r} \quad [3]$$

$$K(h)=K_{sat}\left[S_e(h)\right]^l\left\{1-\left\{1-\left[S_e(h)\right]^{1/m}\right\}^m\right\}^2 \quad [4]$$

$$m=1-\frac{1}{n} \quad [5]$$

where θ_r and θ_s are the residual and saturated water content, respectively, l is a tortuosity factor (held at 0.5 for this experiment), n and α are fitting parameters, S_e is the effective water content, and K_{sat} and K are the saturated and variably saturated hydraulic conductivities, respectively, for each soil layer. These parameters, θ_r, θ_s, n, α, and K_{sat}, which are unique for each soil texture, comprise the SHP estimated in the inversion. Reference van Genuchten–Mualem parameters were extracted from the Rosetta database (Schaap et al., 2001) (Supplemental Table S2) corresponding to the sand, silt, and clay contents in each layer and were input to the HYDRUS model.

The one-dimensional HYDRUS model was run hourly for 12 mo starting in November 2009 and spatially discretized at 0.02-m intervals to a depth of 1 m, then increasing geometrically by a factor of 1.25 to a depth of 6 m, for a total of 73 vertical nodes. The lower and upper boundaries of the model were controlled by free drainage and atmospheric conditions, respectively. Hourly precipitation and air temperature inputs to HYDRUS were obtained from an adjacent Michigan EnviroWeather Network station at the Long-term Ecological Research site (Fig. 4). Each HYDRUS simulation, for the reference, sensitivity, and test scenarios, was initialized with the same soil moisture distribution, which reflects realistic field conditions for the model start date.

Once the hydrological modeling was complete, static geophysical models were created at the desired sampling frequency (survey dates are shown on Fig. 4). The geophysical modeling consists of three steps (Fig. 1): (i) converting simulated soil moisture to ER at a standard temperature (25°C), (ii) correcting for distributed subsurface temperatures on the survey date (Fig. 4), and (iii) forward-simulating the potential field for a synthetic ER survey. These steps were repeated for each survey date comprising the ER dataset.

Laboratory resistivity experiments were run to calculate an empirical relationship between soil moisture and ER measurements. Sample material was placed in a 22.2- by 4- by 3.2-cm soil

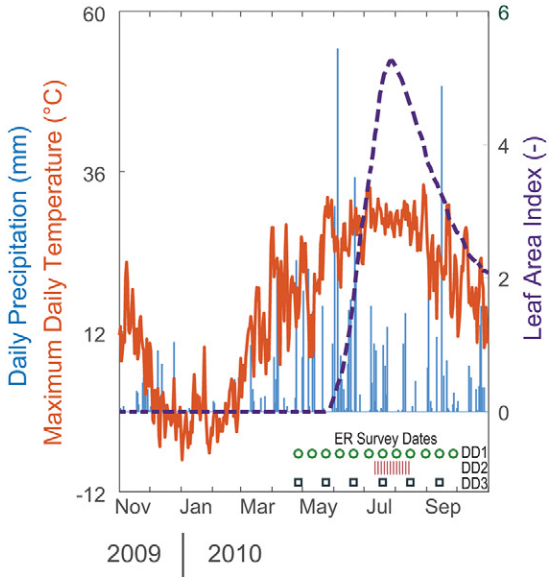

Fig. 4. Measured maximum daily air temperature (orange) and daily precipitation (blue), with SALUS-modeled leaf area index (purple) throughout the model year. The electrical resistivity (ER) survey dates comprising the synthetic datasets for the data density scenarios (DD1, DD2, and DD3) are marked in the bottom right. All site characterization scenarios as well as the sensitivity analysis share the same survey dates with DD1.

box with metal plates for current transmission at the far ends. The resistance was measured using two electrodes near the center of the box while gradually increasing the water content in the sample (see details of this laboratory approach in Jayawickreme et al., 2010). This was repeated for nine soil samples, collected from each of the three soil layers at three adjacent plots. The power-law petrophysical relationship was fit to the observations for each nth soil layer (Supplemental Fig. S1):

$$\rho_x = a_n \theta_x^{-k_n} \quad [6]$$

where ρ_x is the resistivity at depth x, θ_x is the water content at depth x, and a_n and k_n are soil-specific empirical PP.

For this study, we made the simplifying assumption that there was no additional grain surface conductivity term in the petrophysical relationship for any soil layer. Given the frequency of precipitation events that flush out salts accumulated through evapotranspiration, we also assumed that the pore-water conductivity did not undergo changes with time (Jayawickreme et al., 2010). However, this coupled inversion could be modified to incorporate solute transport within the hydrological model, allowing the petrophysical relationship to be transient.

Subsurface resistivity is temperature dependent, thus it is important to account for the belowground temperature gradient. The site was also instrumented with high-temporal-resolution (every 2 h) temperature sensors (Thermochron iButton DS1922L) at three depths (0.26, 0.66, and 1.20 m). We generated realistic soil temperatures for the synthetic study using a heat transport model for soil temperatures at all nodes. Heat transport parameters (Supplemental Table S4) for the Chung and Horton soil temperature model (Chung and Horton, 1987) in HYDRUS were calibrated using soil and air temperature data from February to May 2010. The parameters were iteratively estimated for Layers 1, 2, and 3, consecutively, with the HYDRUS model (non-growing season only) in inversion mode. The ER modeled at the standard 25°C was corrected to the ER at the modeled temperature T for each node x using the linear model from Hayley et al. (2007):

$$\rho_{x_T} = \rho_{x_{25}} \left[\frac{1}{0.0183(T_x - 25) + 1} \right] \quad [7]$$

Once the temperature-corrected ER distribution is calculated, a synthetic ER survey can be modeled. The electrode array used to generate the synthetic data mirrors the installation at the Kellogg Biological Station site and is comprised of 30 surface electrodes spaced 0.3 m apart. This array length was chosen to focus on the upper 2 m of the profile. Due to the assumptions about lateral homogeneity in the model, the 13 unique electrode geometries in dipole–dipole configuration were modeled with the FW2_5D code (Pidlisecky and Knight, 2008), creating a one-dimensional profile of effective measurement depths. The electrical potential field forward modeling code, FW2_5D, allows the input ER distribution to vary in the x and z directions, assuming homogeneity in the y direction. Because our hydrological model varied only in the z direction, we extrapolated our calculated one-dimensional ER laterally. The FW2_5D model was discretized such that errors for our electrode array were 0.7% on average from the analytical solution for a homogenous Earth, yet still efficient. The x dimension grid spacing was 0.15 m (half the distance between electrodes) across the span of the center of the model, increasing by a factor of two in each direction from the center for a total model length of 24 m. The vertical discretization was the same as that described for the HYDRUS model above.

To complete the coupled hydrogeophysical inversion, we use the synthetic ER data from each survey to estimate the SHP, PP, and RP through optimization. The robust SCE-UA global optimization algorithm minimizes an objective function Φ:

$$\Phi = \sqrt{\frac{\sum (V_{\text{meas}} - V_{\text{mod}})^2}{n}} \quad [8]$$

between the modeled (V_{mod}) and "measured" (V_{meas}) synthetic ER data by evolving the coupled model parameters. Because the soil moisture profile output from the hydrological model is updated with each optimization iteration, the soil ER distribution also changes according to the petrophysical model. This in turn alters the modeled potential field and therefore the modeled ER data. This optimization continues until the resulting modeled ER data match the measured ER data within the optimization specified closure criteria. The SCE-UA blends several traditional optimization approaches to efficiently find the global minimum. It starts by randomly sampling a large population from the parameter space. This population is then divided among a number of complexes,

which each evolve independently toward a minimum. After a given number of evolutions, the complexes shuffle, divide, and begin evolving again. This is repeated until convergence is reached. The size of the population and the number of complexes can be scaled with the complexity of the problem.

Synthetic Experiments

To test the ability of the coupled hydrogeophysical inversion algorithm to estimate SHP, PP, and RP from ER data, we created synthetic ER datasets using a single forward run of the reference model. The reference inputs and parameters used to make the synthetic data were then assumed to be the "true" values in subsequent analyses. To increase the difficulty of the optimization, randomly distributed noise (±0.5%) was added to all synthetic ER data. This relatively low amount of error was chosen so that the impact of the tested data density and parameter error would be clearer. It also reflects the low amount of error (median 0.12%) that was observed between reciprocal measurements for this array in preliminary data analysis from the field site. We next tested the sensitivity of a biweekly (every 2 wk) ER survey dataset to each parameter. Finally, we conducted a series of inversion experiments to retrieve the reference SHP, PP, and RP via iterative optimization starting from some perturbed initial estimate of those parameters.

Parameter Sensitivity

To determine which parameters to estimate, which to fix, and how to perturb parameters for each inversion scenario, we conducted a sensitivity analysis using forward runs of the algorithm. Univariate "one-dimensional" sensitivity was tested for each of the SHP, RP, and PP. Recognizing that some co-dependency exists between parameters, particularly with α (Huisman et al., 2010, Moreno et al., 2015), we expected the global optimization algorithm to overcome this in minimizing the objective function. For this analysis, the algorithm was run sequentially 20 times for each parameter, with values distributed evenly across a predetermined parameter space, while the rest of the parameters were held fixed at their reference values. The ER data selected to test the sensitivity was a biweekly dataset extracted from the reference model run at a 14-d interval from late April 2010 through September 2010 for a total of 12 surveys, comprising 13 measurements each (156 measurements). We quantified the sensitivity of each tested value by computing the root mean square error (RMSE) between the reference synthetic ER data and the perturbed ER data modeled at the same biweekly frequency.

The upper and lower limits for each parameter space (Supplemental Table S2) were chosen based on either (i) physical limits for parameters with narrow realistic ranges such as with n, α, θ_r, and θ_s (Schaap et al., 2001) or (ii) fixed ranges from the reference for parameters with greater variability. For example, upper and lower bounds for K_{sat} were set plus or minus two orders of magnitude around the reference value, given the large uncertainty of that parameter. The petrophysical parameter limits were set ±10% the value used in the reference run based on the variability observed in the field data (Supplemental Fig. S1). Limits on the Feddes RP were set to ±30% of the reference value to see if sensitivity to those parameters existed at levels beyond what has been previously tested (perturbation of 1% in Hupet et al., 2003). Bounds for pz were chosen to allow the "effective" MRD to vary from 0.5 to 1.5 m.

Sensitivity Analysis Results

The results from the sensitivity analysis show that as parameters deviated from their reference values, the RMSE between the reference ER data and the perturbed ER data increased nearly linearly (Fig. 5). The SHP from the first soil layer were significantly more sensitive than those from deeper layers, with the exception of α, which had only slightly increased sensitivity in the first layer. As in prior research (Mboh et al., 2012), we found very little sensitivity to the Feddes RP relative to the SHP with the exception of h_4. This was not surprising because h_4 controls the point at which RWU ceases under very dry conditions. However, we observed that the RP pz had roughly the same sensitivity as the PP (note that pz had a much larger parameter space).

A threshold RMSE value (Eq. [8]) of 0.1 was chosen to isolate the highest sensitivity parameters from the rest, which included

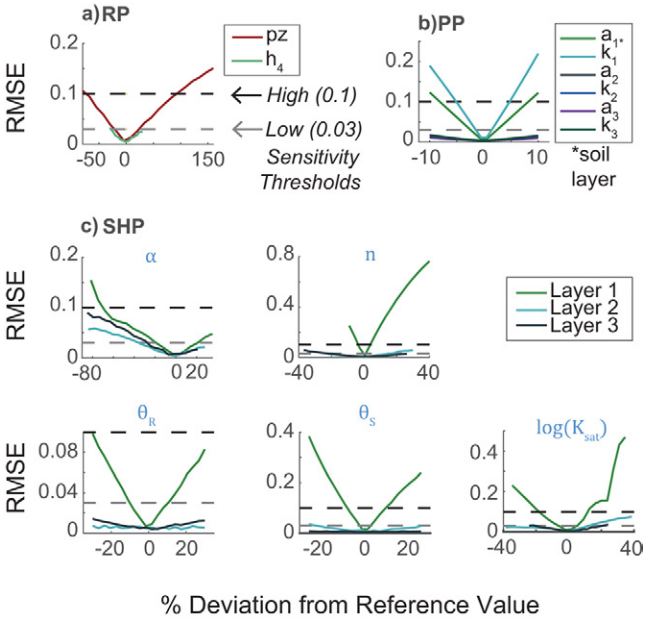

Fig. 5. Sensitivity analysis results for (a) root parameters (RP), including the Vrugt equation (Eq. [1]) root distribution parameter, pz, and the Feddes model parameter h_4; (b) petrophysical parameters (PP), including Archie's equation (Eq. [6]) fitting parameters, a_i and k_i; and (c) soil hydraulic parameters (SHP), including van Genuchten–Mualem equation (Eq. [2]) fitting parameters n_i and α_i, saturated hydraulic conductivity $K_{sat,i}$, saturated volumetric water content $\theta_{s,i}$, and residual volumetric water content $\theta_{r,i}$ for layers = 1 to 3. The two sensitivity thresholds at 0.03 and 0.1 are shown as horizontal gray and black dashed lines, respectively. Note that the y scale for root mean square error (RMSE) varies by parameter. The range of tested values corresponds to the upper and lower limits used in the parameter estimation, which varies by parameter. Most RP had no sensitivity in the tested range and are not shown.

all the SHP and PP from the first soil layer. The eight high-sensitivity parameters that fell into this category included the SHP n_1, α_1, $K_{sat,1}$, $\theta_{r,1}$, and θ_{s1}, the PP a_1 and k_1 (numerical subscripts denote soil layers 1, 2, and 3, where applicable), and the RP pz. A secondary threshold of 0.03 was chosen to include the remaining parameters that had lower sensitivity. This category also included eight parameters: for SHP, $n_{2,3}$, $\alpha_{2,3}$, $K_{sat,2,3}$, $\theta_{s,2}$, and the RP h_4. The remaining RP (all Feddes except h_4, not shown), the SHP $\theta_{r,2,3}$ and $\theta_{s,3}$, and the PP $a_{2,3}$ and $k_{2,3}$ were determined to have essentially no sensitivity because perturbing them had no discernible effect on the simulated ER values.

Inversion Scenarios

To test the ability of the inversion to estimate the SHP, PP, and RP under different conditions, we evaluated a suite of six synthetic data inversion scenarios. These experiments were designed to test the robustness of the parameter estimation to decreasing data quality and quantity. We compared model output and parameter estimates for inversions using three data density (DD) types, plus three levels of site characterization (SC) with the same data density.

To test the dependence of the optimization on data density, we created three scenarios mimicking three frequencies of field surveys (Fig. 4). The first scenario, DD1, tested a relatively long-term (6-mo) ER dataset, with moderate survey frequency (biweekly). The dataset for DD1 was used for the parameter sensitivity analysis discussed above and all three SC scenarios (described below); it has 12 surveys with 13 measurements each, for a total of 156 measurements from April to September.

A second scenario, DD2, tested a short-term (1-mo) high-frequency (every 3 d) ER dataset to simulate the effect of using data exclusively from the peak growing season but spanning less diverse seasonal weather conditions. This dataset covers a large precipitation–infiltration event, along with the subsequent transpiration-dominated drying period. The data were extracted from the reference run at a 3-d interval for the period from July to August 2010, for a total of 12 surveys, again comprised of 13 measurements each (156 measurements total).

A third scenario, DD3, tested the effectiveness of a lower frequency (monthly) ER dataset during the same 6-mo period as the dataset in DD1. The data for this scenario were extracted from the reference run at a 4-wk interval, for a total of six surveys with 13 measurements each (78 total measurements). This dataset is half the size of the other two DD scenarios. In all three DD scenarios, the eight highest sensitivity parameters were estimated, while the remaining low- and no-sensitivity parameters were fixed at their reference values.

To test the robustness of the model to various levels of site characterization, we again estimated the high-sensitivity parameters but introduced varying levels of error into the other parameters. These three scenarios included SC1, where the low- and no-sensitivity parameters were assumed well known and were fixed with minimal error (1.5–40%) relative to reference values; SC2, where these parameters were moderately well known and fixed with higher error (2.8–81%); and SC3, where the low-sensitivity parameters were assumed completely unknown and were included in the parameter estimation along with the high-sensitivity parameters. In this scenario, the no-sensitivity parameters were fixed at their reference values. All three SC scenarios used the same synthetic dataset with biweekly ER surveys as that in DD1. In each of the six scenarios, the same starting values were used for the high-sensitivity parameters being estimated. With the exception of θ_r, θ_s, and the PP parameters a and k, which were started at ±5%, all other parameters were started ±30% away from the reference value.

To determine how much fixed error to add to the low-sensitivity SHP for SC1 and SC2, we considered the uncertainty in estimating each parameter of the retention function with standard field methods. This was analyzed by Baroni et al. (2010), who provided a table of standard deviations for each parameter of a three-layer soil. We used the standard deviation from soil Layer 3 in their analysis, which was most similar to the sandy soils at our site. For the PP in our model, we calculated the standard deviation across the three replicate experiments that were conducted at the study site for parameters a and k in each soil layer.

Both the low- and no-sensitivity parameters were fixed at a value half a standard deviation (for SC1) or a full standard deviation (for SC2) from the reference value. The large variation in uncertainty across parameters meant that some were fixed closer to the reference values than others. For example, in SC2, parameters with less uncertainty, such as n, were fixed 3% away from the reference values, while high-uncertainty parameters like α were fixed 72% away. The fixed values used for these scenarios are shown in Supplemental Table S2.

Scenario SC3 tested the feasibility of estimating both the high- and low-sensitivity parameters (a total of 16). This last scenario was designed to replicate the most likely field scenario, where without conducting a relatively intensive laboratory bench experiment, no a priori information would be available for the SHP. The goal was to determine if the inversion algorithm was robust to local minima from the large number of unknowns. If so, the most critical parameters affecting root water dynamics and water fluxes would still be accurately estimated.

For the SCE-UA algorithm, we selected a number of complexes almost equal to the number of unknowns. For all scenarios except SC3, seven complexes were used. Optimization continued until five consecutive shuffles (~200 iterations each) did not improve the objective function by 0.1%. The convergence criterion was generally met after ~4000 iterations. The number of complexes in the SCE-UA algorithm was doubled to 14 for the SC3 scenario due to the larger number of free parameters. In that case, the stopping criteria of 10,000 iterations was reached before convergence; however, three consecutive shuffles had not improved the objective function at that point. Final estimated parameter values and model outputs were from the iteration with the lowest objective function value.

Our study was particularly interested in root water dynamics and therefore we chose to quantify the success of our approach

with four outputs from HYDRUS that capture the root fraction with depth, the cumulative RWU, the soil-water retention function (Eq. [2]), and transient soil moisture. Each inversion scenario was validated by calculating the RMSE between the synthetic model and the hydrologic model with estimated parameters.

Results and Discussion

The capability of the hydrogeophysical inversion algorithm is graphically illustrated in Fig. 6. For this figure, scenario SC3 was chosen to best demonstrate the robustness of the algorithm when all 16 parameters were estimated. The impact of the initial conditions on the root water and soil moisture dynamics can be observed in comparison to the reference model in Fig. 6. The hydrological model with the starting values has a deeper root distribution, more RWU, and a steeper water retention curve. Regardless of the significant error in the starting values, the inversion algorithm estimated the root dynamics and the soil moisture curve well, even prior to the start of the ER surveys.

Regardless of the scenario, there was excellent agreement between the reference and optimized model output (Fig. 7; Table 1). Even in cases where the fixed error in other SHP and RP was large, the inversion found a unique solution for the root distribution within 10% of the reference distribution. We also observed that the cumulative RWU was estimated within 0.01 m for all scenarios with the exception of SC2, which was off by 0.015 m (Fig. 7). The transient soil moisture distribution was also closely matched, despite some nonuniqueness in the SHP. We observed no residuals greater than 0.05 cm^3 cm^{-3} water content, even in the worst performing scenario, SC2 (Fig. 7). The soil-water retention function, which is calculated with the estimated SHP (except K_{sat}, which is not used to calculate soil-water retention), was also estimated within 0.02 cm^3 cm^{-3} of the reference model for each scenario. In Scenario SC3, the SHP perturbed by 30% to start were estimated within 5% of their reference value with the exception of α. In Layers 2 and 3, α did not have a strong sensitivity, improving only to 28%, while in Layer 1 it was improved to 15% from the reference value. The value of K_{sat} in all layers, however, was estimated very well (within 2% of the reference). The parameter estimation results from Scenario SC3 are reported in Supplemental Table S1. The optimization was most sensitive to the soil moisture distribution, and although some parameters were not estimated exactly, the soil water retention function (Fig. 7) and hydraulic conductivity, K_{sat}, were well matched.

We calculated uncertainty in each estimated parameter by calculating the ±1 standard deviation in the parameters from the iterations with 80% or more improvement in the objective function (Vrugt et al., 2003). Table 2 shows the parameter uncertainty for the eight high-sensitivity parameters from Scenario SC3. Most were estimated within ±1 standard deviation of the reference value. The uncertainty in parameter estimates for the other five scenarios, and the low-sensitivity parameters from SC3, can be found in the supplemental material (Supplemental Table S1). The low-sensitivity parameters estimated in SC3 were all estimated within ±1

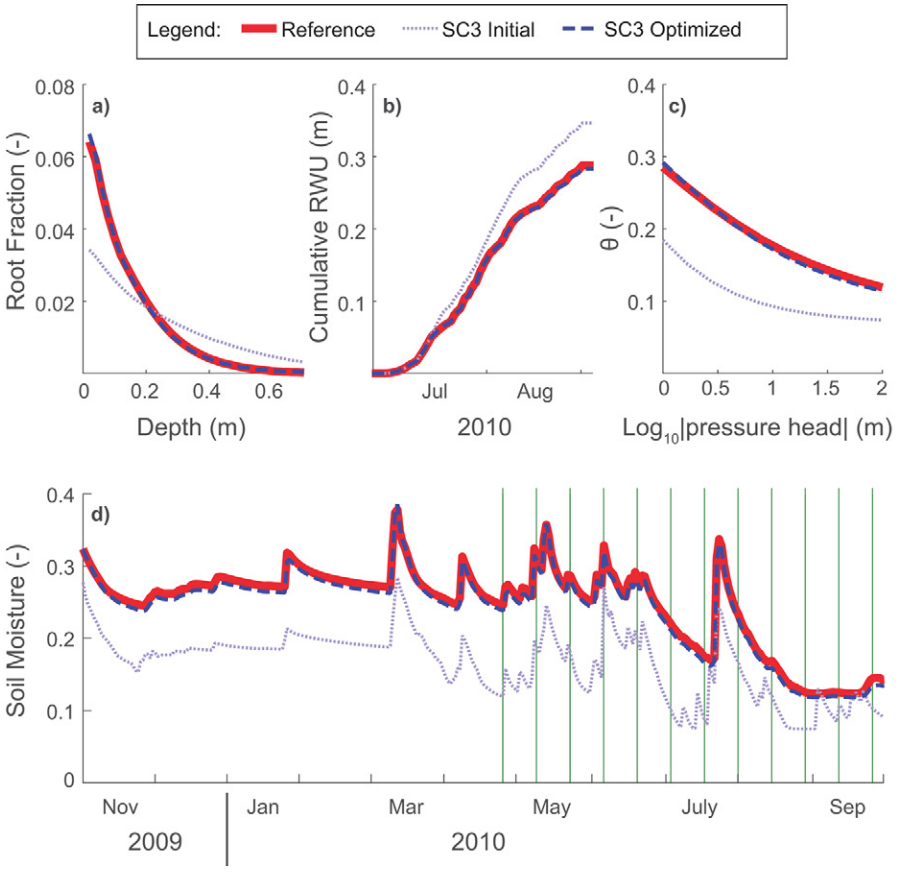

Fig. 6. HYDRUS output for (a) root fraction, (b) root water uptake (RWU) during the growing season, (c) the van Genuchten–Mualem model retention curve, and (d) soil moisture (θ) at 0.2 m with electrical resistivity survey dates for site characterization Scenario 3 (SC3) in green. The estimated values from SC3 are plotted vs. initial values and reference values. The results from the other five scenarios were very similar to SC3 and are not shown here. Note that the HYDRUS outputs were not used in the parameter estimation process, rather they were used only to validate the approach.

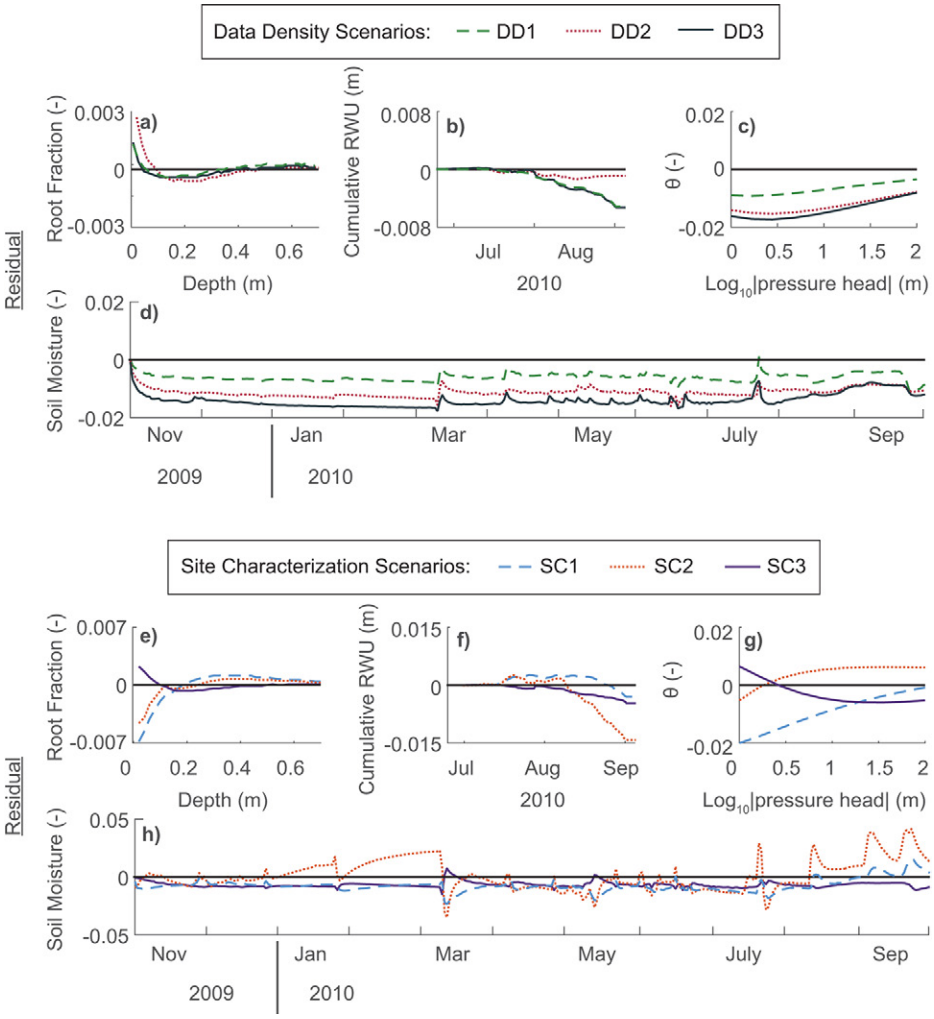

Fig. 7. Residuals of root fraction, root water uptake (RWU), van Genuchten–Mualem model retention curve, and soil moisture (θ) at 0.2 m for (a–d) data density and (e–h) site characterization (SC) scenarios. The low residuals for all scenarios show that there was agreement with the reference values; SC1 and SC2 generally had higher residuals. Note the *y* axis range differences.

standard deviation of the reference value except α_2 and α_3. The uncertainty in the 16 estimated parameters from Scenario SC3 is shown graphically in Supplemental Fig. S2 and S3. Each scenario converged to generally the same result, despite varying the number of estimated parameters and imposed error.

In the DD tests, the model was robust to the quantity and timing of the data used in the objective function. The high-temporal-frequency data (DD2) covered only one large infiltration and subsequent drying event but was still able to estimate the SHP quite well and provided the best estimate of the RWU. This is likely due to the fact that RWU was dominant during the period covered by the data. However, a month-long dataset too early in the growing season may not capture later RWU since there would be no sensitivity to the mature root distribution.

We found that even with half as much data (DD3), results were still good, indicating that the approach would likely be successful even if data collection opportunities were limited by travel, time, or equipment constraints. While six datasets is very sparse compared with the daily or hourly water content data typically used in hydrological inversions such as Moreno et al. (2015), we found it sufficient for this purpose. The first scenario (DD1), with moderately spaced data across the entire growing season, otherwise yielded the best fit of the root distribution and soil moisture, indicating that a longer term dataset at frequent intervals is preferable to a shorter or sparser one.

In the SC tests, we introduced parameter error to the inversion. As expected, even low error was detrimental to the estimation of the high sensitivity parameters, particularly for pz and α, with SC1 being among the worst across all three metrics (Table 1). Higher fixed error in SC2 led to the highest RMSE in two metrics and the second highest in the third and limited reduction in the objective function. Despite this, the root distribution, RWU, and soil moisture matched the reference model quite well, although with generally higher residuals than the DD scenarios (Fig. 7). The soil moisture dynamics of the first layer were not highly dependent on the dynamics of the layers below and were thus still able to be well estimated by the inversion.

While increasing the number of parameters in the SCE algorithm for SC3 slowed the convergence time by a factor of four, we observed that the algorithm did a much better job estimating the high-sensitivity parameters than in the scenarios with fewer free parameters but with fixed parameter error (SC1 and SC2). As observed by Hupet et al. (2003), despite the low sensitivity of the SHP in Layers 2 and 3, fixing these properties at incorrect values considerably impeded the algorithm from reducing the objective

Table 1. Root mean squared error (RMSE, multiplied by a factor of 100 for display purposes) between the reference and optimized estimates of the root distribution, daily soil moisture in Layer 1 (at 0.2 m), and cumulative root water uptake (RWU). Superscripts are used to rank each scenario within that metric (1 being the best fit).

Scenario	Root distribution	Soil moisture	RWU
Data density scenarios			
DD1–2 wk data	0.0314^{1}	0.642^{1}	0.424^{2}
DD2–3 d data	0.0554^{4}	1.16^{3}	0.226^{1}
DD3–4 wk data	0.0336^{2}	1.44^{5}	0.505^{3}
Site characterization scenarios			
SC1–low error in low-sensitivity parameters	0.177^{6}	1.34^{4}	0.714^{5}
SC2–high error in low-sensitivity parameters	0.116^{5}	1.60^{6}	1.60^{6}
SC3–estimate low-sensitivity parameters	0.0489^{3}	0.844^{2}	0.544^{4}

Table 2. Uncertainty in the eight high-sensitivity parameters estimated in site characterization Scenario SC3: the petrophysical parameters (PP) from Layer 1, Archie's equation (Eq. [6]) fitting parameters a_1 and k_1; the root parameter (RP), Vrugt equation (Eq. [1]) parameter pz; and the soil hydraulic parameters (SHP) from Layer 1, van Genuchten–Mualem equation (Eq. [2]) fitting parameters n_1 and α_1, saturated hydraulic conductivity $K_{sat,1}$, saturated volumetric water content $\theta_{s,1}$, and residual volumetric water content $\theta_{r,1}$. We calculated the standard deviation (σ) in parameters from the iterations with >80% improvement in objective function. Most high-sensitivity parameters were estimated within $\pm 1\sigma$ of the reference value.

Parameter	Reference	SC3 estimate	Mean	σ
PP				
a_1	16.21	16.29	16.26	0.34
k_1	1.01	0.99	0.98	0.020
RP				
pz	8.14	8.66	8.34	1.29
SHP				
n_1	1.32	1.37	1.38	0.06
α_1	2.70	2.29	2.25	0.37
$\log(K_{sat,1})$	−5.79	−5.87	−5.80	0.37
$\theta_{s,1}$	0.39	0.40	0.40	0.021
$\theta_{r,1}$	0.066	0.071	0.070	0.004

function (Table 1). In contrast, allowing those parameters to be estimated in concert with the high-sensitivity parameters resulted in a better fit of the root and soil moisture dynamics (Fig. 6; Table 1). The optimization algorithm was robust to the large number of unknowns in this scenario.

We note that SC3 also improved the soil moisture estimates in Layer 1 from DD2 and DD3 and the root distribution estimate from DD2 (Table 1). This indicates that the timing of the data played a role, as we observed that every other week data with estimated low-sensitivity parameters (SC3) performed better than sparser data with perfect low-sensitivity parameters (DD2 and DD3). This is likely because this dataset captured the greatest variety of soil moisture regimes. This scenario was also able to estimate parameters in all three types of soil present at the Kellogg Biological Station field site, indicating that this approach is not as limited by texture or depth as was expected.

Contrary to Hupet et al. (2003), we did not observe a limitation in parameter estimation capacity for the medium-fine textured first soil layer. We imposed a small amount of error in the ER data but assumed that model features such as layer boundaries and basic climate inputs would be easy to obtain at the field scale and thus were held fixed at the reference values for this study. Hinnell et al. (2010) concluded that results with low residuals, as presented here, are likely only obtainable with a physically representative hydrological model, and future work should explore those limitations. Our results show that even with large parameter bounds and conservative starting values for the SHP, the soil moisture and root dynamics could be estimated accurately.

Conclusions

In this study, we developed and validated the use of a novel hydrogeophysical inversion algorithm to estimate SHP, PP, and RP simultaneously for a multilayered soil. Our results indicate that this is a promising approach. Through the accurate estimation of parameters that control root and soil moisture dynamics within the coupled hydrogeophysical model, the synthetic transient root and soil moisture distributions across a variety of data densities and site characterization scenarios were retrieved. This suggests that transient soil moisture processes depend on a *unique* root distribution, which is critical because it is very difficult to independently measure the effective root distribution in a field setting. While prior research has studied the use of direct soil moisture data to inversely estimate root parameters, we found that data from a simple ER electrode array collected during part of the growing season was capable of the same, even when errors were present in the petrophysical relationship and data were more limited. Relative to approaches that use water content data for the hydrological inversion, the ER data was temporally sparse, yet this did not prove to be a limitation. The high spatial coverage achievable with this noninvasive approach appears to be as useful for capturing root water dynamics. The approach was very successful in the most realistic scenario (SC3), with poor a priori site characterization of the three soil layers and many unknown parameter values. This methodology provides a minimally invasive and cost-effective approach to better understand root water dynamics in a variety of settings. This is a promising result for the study of perennial and/or deep root systems that are particularly difficult to characterize with traditional methods.

While a realistic field setting can be expected to contain varied topography, soil heterogeneities, and larger root systems, ER data are well suited to capture such variability. The capabilities of modern computing and robust parameter estimation algorithms make it possible to model increasingly complex

systems. Future work will expand to two and three dimensions to take full advantage of ER's ability to image spatial and temporal changes at the field scale. With the successful validation of the method that identified a unique transient root distribution, we plan to repeat the inversion with ER data from the Kellogg Biological Station Great Lakes Bioenergy Research Center field site for a variety of biofuel crops.

Acknowledgments

This research was funded by National Science Foundation Grants EAR-0911642 and 1039180 and the USDA NIFA Water CAP Grant 2015-68007-23133. Any opinions, findings, and conclusions or recommendations expressed in this publication are those of the authors and do not necessarily reflect the views of the NSF or USDA. We thank Kaya Diker for providing the petrophysical laboratory measurements (Supplemental Fig. S1) and the Great Lakes Bioenergy Research Center for providing the soil textural data used in this research. We would also like to thank Sarah Garré and one anonymous reviewer for their constructive comments that helped to improve the manuscript.

References

Amato, M., B. Basso, G. Celano, G. Bitella, G. Morelli, and R. Rossi. 2008. In situ detection of tree root distribution and biomass by multi-electrode resistivity imaging. Tree Physiol. 28:1441–1448. doi:10.1093/treephys/28.10.1441

Archie, G.E. 1942. The electrical resistivity log as an aid in determining some reservoir characteristics. Trans. Am. Inst. Min. Metall. Eng. 146:54–61.

Baroni, G., A. Facchi, C. Gandolfi, B. Ortuani, D. Horeschi, and J.C. van Dam. 2010. Uncertainty in the determination of soil hydraulic parameters and its influence on the performance of two hydrological models of different complexity. Hydrol. Earth Syst. Sci. 14:251–270. doi:10.5194/hess-14-251-2010

Bass, B., M.B. Cardenas, and K.M. Befus. 2017. Seasonal shifts in soil moisture throughout a semiarid hillslope ecotone during drought: A geoelectrical view. Vadose Zone J. 16(2). doi:10.2136/vzj2016.11.0108

Basso, B., J.T. Richie, P.R. Grace, and L. Sartori. 2006. Simulation of tillage system impact on soil biophysical properties using the SALUS model. Ital. J. Agron. 1:677–688. doi:10.4081/ija.2006.677

Beff, L., T. Günther, B. Vandoorne, V. Couvreur, and M. Javaux. 2013. Three-dimensional monitoring of soil water content in a maize field using electrical resistivity tomography. Hydrol. Earth Syst. Sci. 17:595–609. doi:10.5194/hess-17-595-2013

Cai, G., H. Vereecken, V. Couvreur, and C.M. Mboh. 2018. Parameterization of root water uptake models considering dynamic root distributions and water uptake compensation. Vadose Zone J. 17(1). doi:10.2136/vzj2016.12.0125

Chung, S., and R. Horton. 1987. Soil heat and water flow with a partial surface mulch. Water Resour. Res. 23:2175–2186. doi:10.1029/WR023i012p02175

Duan, Q., S. Sorooshian, and V. Gupta. 1992. Effective and efficient global optimization for conceptual rainfall–runoff models. Water Resour. Res. 28:1015–1031. doi:10.1029/91WR02985

Fan, J., A. Scheuermann, A. Guyot, T. Baumgartl, and D.A. Lockington. 2015. Quantifying spatiotemporal dynamics of root-zone soil water in a mixed forest on subtropical coastal sand dune using surface ERT and spatial TDR. J. Hydrol. 523:475–488. doi:10.1016/j.jhydrol.2015.01.064

Feddes, R.A., H. Hoff, M. Bruen, T. Dawson, P. de Rosnay, P. Dirmeyer, et al. 2001. Modeling root water uptake in hydrological and climate models. Bull. Am. Meteorol. Soc. 82:2797–2809. doi:10.1175/1520-0477(2001)082<2797:MRWUIH>2.3.CO;2

Garré, S., I. Coteur, C. Wongleecharoen, T. Kongkaew, J. Diels, and J. Vanderborght. 2013. Noninvasive monitoring of soil water dynamics in mixed cropping systems: A case study in Ratchaburi Province, Thailand. Vadose Zone J. 12(2). doi:10.2136/vzj2012.0129

Garré, S., M. Javaux, J. Vanderborght, L. Pagès, and H. Vereecken. 2011. Three-dimensional electrical resistivity tomography to monitor root zone water dynamics. Vadose Zone J. 10:412–424. doi:10.2136/vzj2010.0079

Hartmann, A., J. Šimůnek, M.K. Aidoo, S.J. Seidel, and N. Lazarovitch. 2018. Implementation and application of a root growth module in HYDRUS. Vadose Zone J. 17:170040. doi:10.2136/vzj2017.02.0040

Hayley, K., L.R. Bentley, M. Gharibi, and M. Nightingale. 2007. Low temperature dependence of electrical resistivity: Implications for near surface geophysical monitoring. Geophys. Res. Lett. 34:L18402. doi:10.1029/2007GL031124

Hinnell, A.C., T.P.A. Ferré, J.A. Vrugt, J.A. Huisman, S. Moysey, J. Rings, and M.B. Kowalsky. 2010. Improved extraction of hydrologic information from geophysical data through coupled hydrogeophysical inversion. Water Resour. Res. 46:W00D40. doi:10.1029/2008WR007060

Huisman, J.A., J. Rings, J.A. Vrugt, J. Sorg, and H. Vereecken. 2010. Hydraulic properties of a model dike from coupled Bayesian and multi-criteria hydrogeophysical inversion. J. Hydrol. 380:62–73. doi:10.1016/j.jhydrol.2009.10.023

Hupet, F., S. Lambot, R.A. Feddes, J.C. van Dam, and M. Vanclooster. 2003. Estimation of root water uptake parameters by inverse modeling with soil water content data. Water Resour. Res. 39:1312. doi:10.1029/2003WR002046

Jackson, R.B., J. Canadell, J.R. Ehleringer, H.A. Mooney, O.E. Sala, and E.D. Schulze. 1996. A global analysis of root distributions for terrestrial biomes. Oecologia 108:389–411. doi:10.1007/BF00333714

Jasechko, S., Z.D. Sharp, J.J. Gibson, S.J. Birks, Y. Yi, and P.J. Fawcett. 2013. Terrestrial water fluxes dominated by transpiration. Nature 496:347–350. doi:10.1038/nature11983

Jayawickreme, D.H., R.L. Van Dam, and D.W. Hyndman. 2008. Subsurface imaging of vegetation, climate, and root-zone moisture interactions. Geophys. Res. Lett. 35:L18404. doi:10.1029/2008GL034690

Jayawickreme, D.H., R.L. Van Dam, and D.W. Hyndman. 2010. Hydrological consequences of land-cover change: Quantifying the influence of plants on soil moisture with time-lapse electrical resistivity. Geophysics 75(4):WA43–WA50. doi:10.1190/1.3464760

Laloy, E., M. Javaux, M. Vanclooster, C. Roisin, and C.L. Bielders. 2011. Electrical resistivity in a loamy soil: Identification of the appropriate pedo-electrical model. Vadose Zone J. 10:1023–1033. doi:10.2136/vzj2010.0095

Ma, Y., R.L. Van Dam, and D.H. Jayawickreme. 2014. Soil moisture variability in a temperate deciduous forest: Insights from electrical resistivity and throughfall data. Environ. Earth Sci. 72:1367–1381. doi:10.1007/s12665-014-3362-y

Maeght, J.L., B. Rewald, and A. Pierret. 2013. How to study deep roots—and why it matters. Front. Plant Sci. 4:299. doi:10.3389/fpls.2013.00299

Mboh, C.M., J.A. Huisman, N. Van Gaelen, J. Rings, and H. Vereecken. 2012. Coupled hydrogeophysical inversion of electrical resistances and inflow measurements for topsoil hydraulic properties under constant head infiltration. Near Surf. Geophys. 10:413–426. doi:10.3997/1873-0604.2012009

Michot, D., Y. Benderitter, A. Dorigny, B. Nicoullaud, D. King, and A. Tabbagh. 2003. Spatial and temporal monitoring of soil water content with an irrigated corn crop cover using surface electrical resistivity tomography. Water Resour. Res. 39:1138. doi:10.1029/2002WR001581

Minsley, B.J., B.L. Burton, S. Ikard, and M.H. Powers. 2011. Hydrogeophysical investigations at Hidden Dam, Raymond, California. J. Environ. Eng. Geophys. 16:145–164. doi:10.2113/JEEG16.4.145

Moreno, Z., A. Arnon, and A. Furman. 2015. Hydro-geophysical monitoring of orchard root zone dynamics in semi-arid region. Irrig. Sci. 33:303–318. doi:10.1007/s00271-015-0467-3

Pidlisecky, A., and R. Knight. 2008. FW2_5D: A MATLAB 2.5-D electrical resistivity modeling code. Comput. Geosci. 34:1645–1654. doi:10.1016/j.cageo.2008.04.001

Richards, L.A. 1931. Capillary conduction of liquids in porous mediums. J. Appl. Phys. 1:318–333. doi:10.1063/1.1745010

Ritchie, J.T. 1998. Soil water balance and plant water stress. In: G.Y. Tsuji et al., editors, Understanding options for agricultural production. Kluwer Acad. Publ., Dordrecht, the Netherlands. p. 41–54. doi:10.1007/978-94-017-3624-4_3.

Robinson, J.L., L.D. Slater, and K.V.R. Schäfer. 2012. Evidence for spatial variability in hydraulic redistribution within an oak–pine forest from resistivity imaging. J. Hydrol. 430–431:69–79. doi:10.1016/j.jhydrol.2012.02.002

Schaap, M.G., F.J. Leij, and M.Th. van Genuchten. 2001. ROSETTA: A computer program for estimating soil hydraulic parameters with hierarchical pedotransfer functions. J. Hydrol. 251:163–176. doi:10.1016/S0022-1694(01)00466-8

Schelle, H., S.C. Iden, J. Fank, and W. Durner. 2012. Inverse estimation of soil hydraulic and root distribution parameters from lysimeter data. Vadose Zone J. 11(4). doi:10.2136/vzj2011.0169

Šimůnek, J., M.Th. van Genuchten, and M. Šejna. 2005. The HYDRUS-1D software package for simulating the movement of water, heat, and multiple solutes in variably saturated media. Version 3.0. HYDRUS Softw. Ser. 1. Dep. of Environ. Sci., Univ. of Calif., Riverside, Calif.

Singha, K., F.D. Day-Lewis, T. Johnson, and L.D. Slater. 2015. Advances in interpretation of subsurface processes with time-lapse electrical imaging. Hydrol. Processes 29:1549–1576. doi:10.1002/hyp.10280

Tardieu, F. 1988. Analysis of the spatial variability of maize root density: II. Distances between roots. Plant Soil 107:267–272. doi:10.1007/BF02370556

Thomas, N., K.E. Schilling, A.A. Amado, M. Streeter, and L. Weber. 2017. Inverse modeling of soil hydraulic properties in a two-layer system and comparisons with measured soil conditions. Vadose Zone J. 16(2). doi:10.2136/vzj2016.08.0072

Tran, A.P., B. Dafflon, S.S. Hubbard, M.B. Kowalsky, P. Long, T.K. Tokunaga, and K.H. Williams. 2016. Quantifying shallow subsurface water and heat dynamics using coupled hydrological–thermal–geophysical inversion. Hydrol. Earth Syst. Sci. 20:3477–3491. doi:10.5194/hess-20-3477-2016

van Genuchten, M.Th. 1980. A closed-form equation for predicting the hydraulic conductivity of unsaturated soils. Soil Sci. Soc. Am. J. 44:892–898. doi:10.2136/sssaj1980.03615995004400050002x

Vrugt, J.A., H.V. Gupta, W. Bouten, and S. Sorooshian. 2003. A Shuffled Complex Evolution Metropolis algorithm for optimization and uncertainty assessment of hydrologic model parameters. Water Resour. Res. 39:1201. doi:10.1029/2002WR001642

Vrugt, J.A., J.W. Hopmans, and J. Šimůnek. 2001. Calibration of a two-dimensional root water uptake model. Soil Sci. Soc. Am. J. 65:1027–1037. doi:10.2136/sssaj2001.6541027x

Warren, J.M., P.J. Hanson, C.M. Iversen, J. Kumar, A.P. Walker, and S.D. Wullschleger. 2015. Root structural and functional dynamics in terrestrial biosphere models: Evaluation and recommendations. New Phyt. 205:59–78. doi:10.1111/nph.13034

Wesseling, J.G., J.A. Elbers, P. Kabat, and B.J. van den Broek. 1991. SWATRE: Instructions for input. Internal Note. Winand Staring Centre, Wageningen, the Netherlands.

Whalley, W.R., A. Binley, C.W. Watts, P. Shanahan, I.C. Dodd, E.S. Ober, et al. 2017. Methods to estimate changes in soil water for phenotyping root activity in the field. Plant Soil 415:407–422. doi:10.1007/s11104-016-3161-1

Zenone, T., I. Gelfand, J. Chen, S.K. Hamilton, and G.P. Robertson. 2013. From set-aside grassland to annual and perennial cellulosic biofuel crops: Effects of land use change on carbon balance. Agric. For. Meteorol. 182–183:1–12. doi:10.1016/j.agrformet.2013.07.015